

A High Quality Factor Carbon Nanotube Mechanical Resonator at 39 GHz

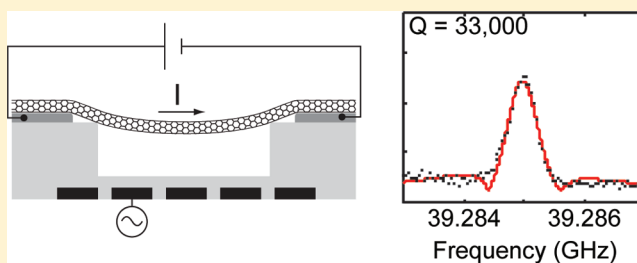
Edward A. Laird, Fei Pei, Wei Tang, Gary A. Steele, and Leo P. Kouwenhoven*

Kavli Institute of Nanoscience, Delft University of Technology, P.O. Box 5046, 2600 GA Delft, The Netherlands

S Supporting Information

ABSTRACT: We measure the mechanical resonances of an as-grown suspended carbon nanotube, detected via electrical mixing in the device. A sequence of modes extending to 39 GHz is observed with a quality factor of 35 000 in the highest mode. This unprecedentedly high combination corresponds to a thermal excited state probability below 10^{-8} and a relaxation time of 140 ns with microsecond relaxation times for lower modes. The effect of electron tunneling on the mechanical resonance is found to depend on frequency as the tunneling time becomes comparable to the vibration period.

KEYWORDS: Nanomechanics, electromechanical devices, carbon nanotubes, quantum dots



Nanomechanical resonators allow the motion of massive objects to be studied in the quantum regime.^{1–5} For quantum behavior to become apparent, a resonator must be cooled with high probability into its ground state, which requires a temperature $T < hf_{\text{res}}/k_B$, where f_{res} is the resonance frequency and h and k_B are, respectively, Planck's and Boltzmann's constants. At the same time, a high quality factor Q is required for a long-lived quantum state. In resonators fabricated by top-down etching,⁶ making a device small to increase f_{res} leads to large surface losses and low Q . These requirements can be reconciled in carbon nanotubes where surface damage is eliminated by growing the nanotube in the final fabrication step.^{7,8} In this Letter, we present a nanotube electromechanical resonator with a harmonic spectrum of modes extending to $f_{\text{res}} = 39$ GHz with $Q > 10\,000$, an unprecedentedly high combination.⁵ Driving the resonances with an on-chip metallic gate creates a measurable signal even at the highest frequencies. Dilution refrigeration to 100 mK implies an excited-state occupation probability of less than 10^{-8} .

The ground state of a mechanical resonator has previously been accessed both by active cooling via sideband coupling to an electromagnetic cavity^{3–5} and passively through dilution refrigeration.² This allowed Fock states of the resonator to be generated through coupling to a superconducting qubit, although the short relaxation time (6 ns) prevented creation of more complex quantum states.² Carbon nanotube resonators^{9–11} have shown very high Q factors^{7,8} below 1.1 GHz. Higher resonances have been identified in transport spectroscopy.^{12,13}

The device studied (Figure 1a) consists of a trench 900 nm wide etched into a layer of plasma-enhanced chemical vapor deposited SiO_2 . Five W finger gates are defined beneath the trench, and W/Pt contacts 40 nm thick are deposited on either side; finally, a nanotube is grown by chemical vapor deposition

to bridge between the two contacts.^{7,8} Electrical measurements were performed in a dilution refrigerator at a mixing chamber temperature of ~ 100 mK with a bias $V_{\text{sd}}^{\text{DC}} = 2$ mV applied across the device. As a function of voltage applied to all gates, the current through the device is close to zero around +0.5 V and increases on either side of this setting, corresponding to conduction via electrons and holes (Figure 1b). Regularly spaced Coulomb blockade peaks show that a quantum dot is defined in the nanotube with an addition energy measured to be ~ 7 meV. This is somewhat smaller than in other suspended devices,^{14–16} but as expected given the slightly larger dimensions of this device, and is consistent with a quantum dot formed across the main suspended part of the nanotube.

Mechanical resonances are excited by a microwave voltage with frequency f and amplitude δV_g^0 applied to one of the gates, and detected in the dc current by the following mixing effect:⁹ The oscillating part of the gate voltage $\delta V_g(t) = \delta V_g^0 \cos(2\pi ft)$ drives motion of the nanotube $\delta u(t) = \delta u^0 \cos(2\pi ft + \phi_M)$, where $u(t)$ is the nanotube's displacement, δu^0 the amplitude of the motion, ϕ_M the phase difference between the drive and the motion, and t time. At the same time, the source–drain voltage V_{sd} acquires an oscillating component $\delta V_{\text{sd}}(t) = \delta V_{\text{sd}}^0 \cos(2\pi ft + \phi_E)$ with amplitude δV_{sd}^0 and phase ϕ_E , induced between the leads by capacitive coupling. The conductance through the nanotube $G(V_g, u)$ depends on source–drain and gate voltages as well as on the displacement (via changes in gate capacitance^{7,9,17} or tunnel rates¹⁸) and for small drive voltages can be expanded as $G(V_g(t), u(t)) \approx G_0 + (\partial G/\partial V_g)\delta V_g(t) + (\partial G/\partial u)\delta u(t)$ with G_0 the conductance in the absence of driving. The time-averaged current through the device is therefore

Received: September 20, 2011

Published: November 23, 2011

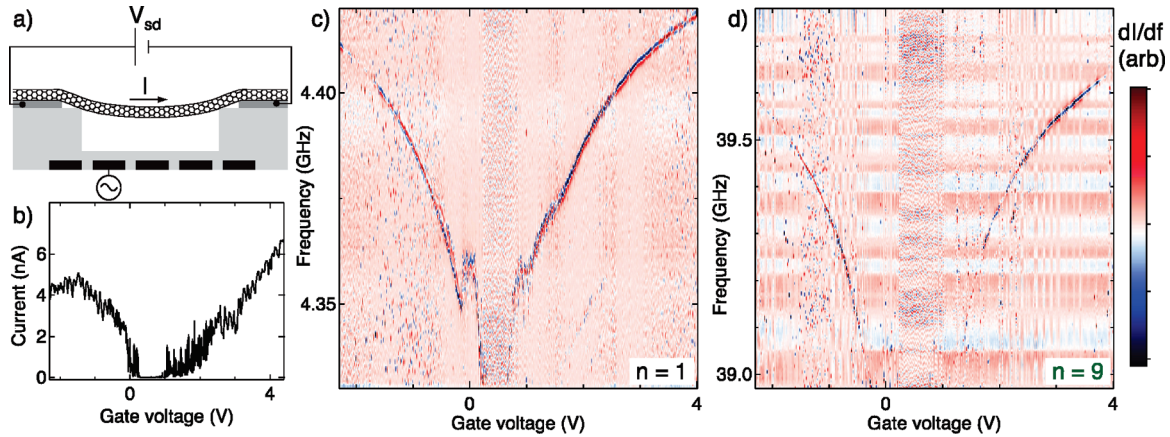


Figure 1. (a) Schematic of the device and measurement circuit. The nanotube is suspended between W/Pt contacts (dark gray) across a trench in an SiO₂ substrate (light gray). The five W gates are shown in black, with the microwave driving voltage applied to the gate indicated. A bias V_{sd} is applied across the device as shown, and the time-averaged current I is measured. (b) Current through the device as a function of dc voltage on all gates with $V_{sd} = 2$ mV. (c,d) Numerically differentiated dI/df as a function of gate voltage and microwave frequency for the fundamental (c) and ninth (d) modes. The mechanical resonances are evident as V-shaped features. (To make the resonances clearer, data has been normalized by standard deviation in each row and column.)

$$\begin{aligned}
 I &= \langle G(t)V_{sd}(t) \rangle \\
 &= G_0 V_{sd}^{DC} + \frac{\delta V_{sd}^0}{2} \left(\frac{\partial G}{\partial V_g} \delta V_g^0 \cos \phi_E \right. \\
 &\quad \left. + \frac{\partial G}{\partial u} \delta u^0 \cos(\phi_E - \phi_M) \right). \tag{1}
 \end{aligned}$$

Resonances are evident as sharp steps in $I(f)$, which arise because on resonance δu^0 is large while ϕ_M changes rapidly as a function of frequency (since the displacement goes from in-phase with the driving below resonance to out-of-phase above resonance.) Numerically differentiating the measured $I(f)$ to make the signal clearer, the resonances are evident as peaks or dips in dI/df . A sequence of such resonances was observed at frequencies up to 39 GHz (see Supporting Information) of which two elements are shown in Figure 1c,d. The mechanical nature of these resonances is confirmed by the gate voltage dependence; larger absolute gate voltages (either positive or negative) pull the nanotube downward, increasing the tension and thus the resonance frequency.^{7,9}

Most of the observed resonances fall into a near-harmonic ladder¹⁰ whose strongest element, which we assign as the fundamental, is at ~ 4.4 GHz (Figure 1c). This is made clear by plotting the normalized resonance frequencies f_n/nf_1 as a function of gate voltage, where f_n is the frequency of the n th mode with $n = 1$ being the fundamental (Figure 2a). A true harmonic spectrum implies $f_n/nf_1 = 1$ for all modes. The observed frequencies fall close to this value but with significant deviations which vary irregularly with n and are largest for the highest modes.

A number of fractional modes were also observed ($n = 1/4, 1/2, 3/2$), which we attribute to parametric driving of the integer modes as the nanotube tension is modulated by the gate voltage.^{19,20} (These are electrically mixed down to a dc signal via higher-order current terms not included in eq 1, such as the current proportional to V_{sd}^4 .) The evidence for assigning the ~ 4.4 GHz resonance as the fundamental, rather than, for example, the ~ 1.1 GHz resonance, is 3-fold. (1) For the same drive power, this resonance is strongest (see below). (2) With

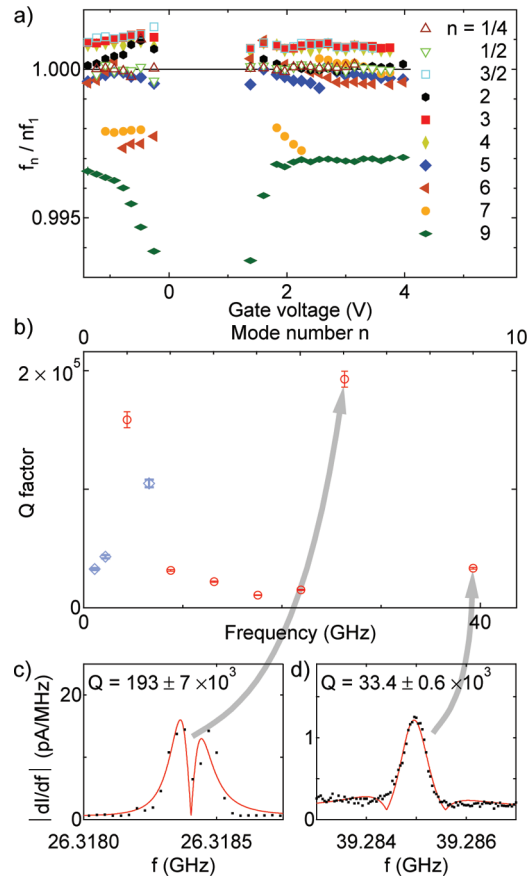


Figure 2. (a) Frequency of each measured mode as a function of voltage on all gates, scaled by mode number and fundamental frequency. All modes fall near but not exactly on the line $f_n = nf_1$ expected for a harmonic sequence. The relative frequency uncertainty is indicated by an error bar (slightly larger than the data point) on the leftmost point of the $n = 9$ series. (b) Highest quality factor measured for selected modes, derived by fitting dI/df as a function of f using eq 2. Error bars indicate the uncertainty of the fits. Integer modes are marked by circles, fractional (parametric) modes by diamonds. (c,d) Data (points) corresponding to two modes in (b), together with the fits (lines) from which the Q factors were derived.

this assignment, nearly all integer modes were observed, but most fractional modes were not (although the entire frequency range was scanned). This is as expected if the fractional modes correspond to weaker parametric resonances, but not otherwise. (3) Consistent with parametric driving, for nearly all the data in Figure 2a the $n = 1/4$ and $n = 1/2$ resonances fall at exact frequency fractions of $n = 1$, while the $n = 3/2$ resonance is at an exact frequency fraction of $n = 3$. However, the elements of the frequency ladder beginning at ~ 4.4 GHz deviate from exact harmonicity, and we therefore exclude the possibility that these resonances reflect parametric driving or purely electrical nonlinearities.

One of the attractive features of nanotube resonators is a large quality factor Q , corresponding to a narrow resonance line width.⁷ For each of the observed modes, Q is determined using a frequency modulation technique.¹⁷ While f is modulated at 59 Hz with depth ~ 10 kHz, the current is monitored using a lock-in amplifier synchronized with the modulation. The magnitude of the lock-in signal at the modulation frequency, $|dI/df|$, shows a peak on resonance, which is numerically fit to obtain Q and f_{res} using the formula (derived in the Supporting Information)

$$\left| \frac{dI}{df} \right| = A \left| \frac{d}{df} \text{Re} \left\{ \frac{e^{-i\varphi_E}}{f_{\text{res}}^2 - f^2 + i \frac{f_{\text{res}} f}{Q}} \right\} \right| + B \quad (2)$$

This follows from eq 1 under the assumptions that the nanotube executes simple harmonic motion and that the frequency dependence comes mainly through the δu^0 and ϕ_M terms, that is, that there is no nearby electrical resonance as sharp as the mechanical resonance. Here A and B are peak scaling and offset, treated as separate fit parameters for each mode.

The fitted Q is shown in Figure 2b for each mode. As seen from Figure 2c,d, the measured $|dI/df|$ as a function of frequency is in good agreement with the form predicted by eq 2. These measurements were made at low powers where the position and width of the peak do not depend on power, thus excluding nonlinear effects such as a Duffing instability.⁷ The quality factor is found to vary irregularly with frequency in the range $10\,000 < Q < 200\,000$, presumably reflecting coupling to different modes of the environment²¹ (Figure 2b). The combination of such high Q and f_{res} has not been previously reported for a mechanical resonator. This data sets a new record for the product Qf_{res} , which characterizes the force sensitivity of the device;²² for the $n = 6$ mode $Qf_{\text{res}} = 5.1 \times 10^{15}$ Hz, more than an order of magnitude larger than previously reported.⁵

We now consider the origin of these very high resonance frequencies. Three limits for transverse vibrations have been identified in which the restoring force arises from residual tension due to fabrication, from gate voltage-induced tension, and from bending rigidity.^{9,23,24} Mechanical resonances are also possible from longitudinal (stretching) vibrations or the radial breathing mode.¹² Each of these possibilities has its own mode spectrum and gate voltage dependence. A harmonic spectrum is consistent only with longitudinal vibrations or with transverse vibrations dominated by residual tension; however, the expected longitudinal frequency for a 900 nm length nanotube, ~ 30 GHz, is much higher than the measured fundamental frequency f_1 .¹² For transverse vibrations, by contrast, the fundamental frequency can take any value depending on the residual tension, and so we ascribe the resonances of Figure 1 to such modes.

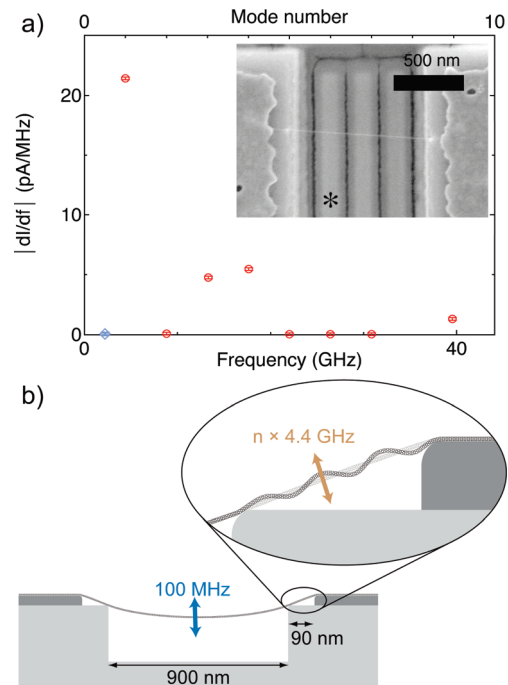


Figure 3. (a) Amplitude of resonance peak for the same driving power at different mode numbers. The error bars indicate the magnitude of electrical noise in the measurement. Integer modes are marked by circles, a fractional mode by a diamond. Inset: top view of device, showing the nanotube stuck to the rim of the trench, creating three suspended segments. The adhesion points are visible in the micrograph as white spots. The gate to which microwaves are applied is indicated by *. (b) Illustration showing two sets of modes coexisting in the same nanotube. A 100 MHz mode corresponds to vibration of the longest segment, while the 4.4 GHz sequence is attributed to one of the shorter segments. In the inset here, $n = 6$.

As can be seen from the inset to Figure 3a, three segments of the nanotube are suspended; the main section over the trench, and two short segments on each side between the rim of the trench and the raised contacts. Each of these can vibrate independently with its own mode structure. As well as the mode sequence shown in Figures 1 and 2, we also observe a resonance at 100 MHz (see Supporting Information) which is presumably due to the longest suspended segment. However, a series of tension modes beginning at 4.4 GHz is incompatible with any lower-frequency resonances in the same segment. We therefore suggest that the modes of Figure 1 correspond to vibrations of a short segment on one side of the trench (Figure 3b). Supporting evidence for this suggestion comes from the fact that a two-dimensional map of current versus gate voltage indicates an incipient quantum dot in one of the leads, whose motion would modulate the overall conductance of the device (see Supporting Information). In this interpretation and estimating the nanotube diameter as ~ 3 nm, the measured $f_1 \approx 4.4$ GHz and suspended length 100 nm imply a residual tension²³ of ~ 6 nN. We note that although the concave dependence of resonance frequency on V_g seen in Figure 1 is qualitatively consistent with a tension mode, at low V_g the frequency decreases more rapidly than the strongest expected dependence, which is $f_{\text{res}} \propto |V_g|^{2/3}$.

The detection of strong mechanical resonances at such high frequencies is surprising, because within a harmonic series the net displacement for the same driving power is expected^{23,25} (for constant Q) to decrease with n^{-4} except for even n , when

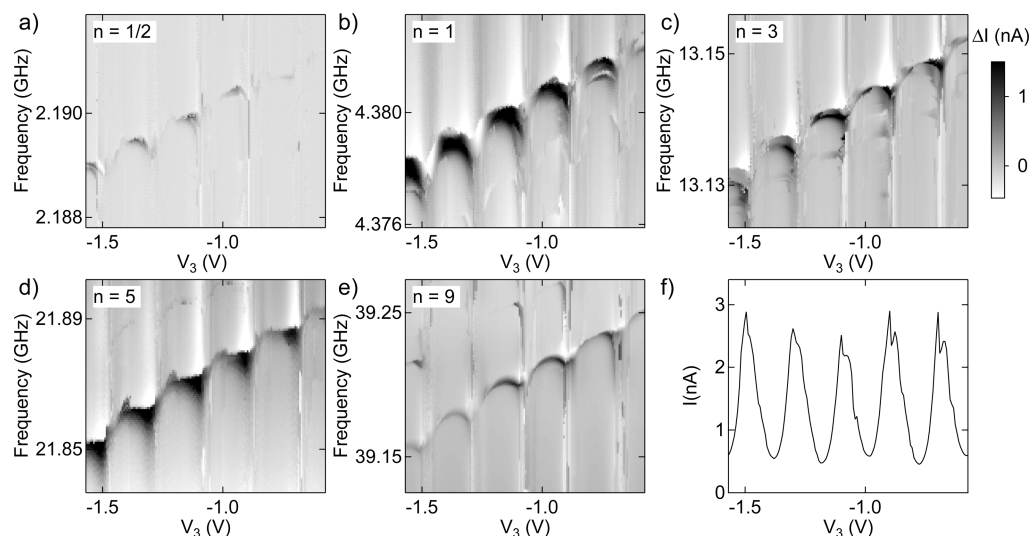


Figure 4. (a–e) Current through the device as a function of V_3 and microwave frequency with the average of each column subtracted. The mechanical resonances show up mainly as a current increase. The resonance frequency is affected by Coulomb blockade in the quantum dot, being roughly constant in each Coulomb valley and decreasing on each Coulomb peak. For higher modes, the on-peak dips are less pronounced. (f) Current as a function of gate voltage with microwaves applied at ~ 1.5 GHz (well away from any mechanical resonance) with the same power as in panel a. The Coulomb peak locations are evident and coincide with the resonance frequency dips in panels a–e.

the net displacement should be zero. Here one power of n^{-1} arises because the restoring force is larger in higher modes, two powers arise because the net displacement is smaller (since different parts of the nanotube move in opposite directions), and one power arises because constant Q implies a larger damping coefficient at higher frequency. To explore this further, in Figure 3a we plot the height of the resonance peaks versus mode number. For all this data, the applied power at the device was approximately equal, calibrated based on the Coulomb peak width (see Supporting Information). Although there is an overall downward trend for the integer modes, the peak height does not fall off as n^{-4} as expected,^{23,25} instead varying strongly between modes, uncorrelated with Q factor. Qualitatively, this irregular variation can arise because the magnitude of the oscillating source–drain voltage δV_{sd}^0 , and hence of I , is affected by the electromagnetic modes of the cryostat. The expected even–odd behavior is partly observed, in that although three of the five odd-integer modes up to $n = 9$ gave a measurable signal at this power, only one out of four even-integer modes did.^{23,25} Even modes are expected to be detected if the dc gate coupling is nonuniform across the vibrating segment, which is likely to be the case if this segment is on one side of the device.

The large number of measurable modes allow us to explore the coupling of mechanical motion and electron tunneling at much higher frequencies than achieved so far.^{8,11} In similar devices, a reduced resonance frequency was observed whenever the quantum dot was tuned close to a Coulomb peak. This was explained by electron tunneling between the dot and the leads, which softens the restoring force by screening changes in the dot's electrical potential as the distance to nearby conductors changes.^{8,11} Such behavior should only be observed if many tunneling events can occur during a single mechanical oscillation, that is, $f_{\text{res}} \ll \Gamma$, where Γ is the tunnel rate. In our device, we are able to test this prediction by measuring for the first time resonance frequencies comparable to Γ . In Figure 4, we show the excess current ΔI due to the mechanical resonance as a function of frequency and dc voltage V_3 on the central gate,

measured for several modes. The other gates were set so that $\Gamma \approx 150$ GHz, measured from Coulomb peak width.^{26,27} The mechanical resonance is detected mainly as an increase in the current. As in previous work,^{8,11} f_{res} is seen to increase in a series of steps coinciding with Coulomb peaks. Each step arises from the extra tension induced in the device by the addition of a single electron, which increases the electrostatic attraction to the gates. The expected dip in frequency is also observed at the Coulomb peaks; however, the gate voltage dependence is not exactly the same between modes. In particular, the dip becomes less strong at the highest frequencies. This is as expected if electron tunneling is softening the restoring force; although the inequality $f_{\text{res}} \ll \Gamma$ is clearly satisfied at 4.4 GHz (and the resulting frequency dips are seen in the data), for the highest modes measured ($n = 5, 9$) the inequality is not so strong, and the dips are correspondingly weakened.

The detection of mechanical modes at such high frequencies is promising for studying mechanical motion in the lowest quantum states.^{1–3} Carbon nanotube devices are particularly attractive in this regard because of their small mass, which leads to a relatively large zero-point motion.⁵ The very large Q factors measured in this work imply long relaxation times, with $T_1 = Q/2\pi f_{\text{res}}$ being 5.8 μs for the $n = 1$ mode and 140 ns for the $n = 9$ mode. Since the quantum coherence time for a mechanical oscillator can be as high as $2T_1$, our data suggest that a carbon nanotube may be suitable for creating complex quantum superpositions of mechanical motion.²

■ ASSOCIATED CONTENT

Supporting Information

Supporting Information includes a derivation of eq 2, a large micrograph of the device, a two-dimensional current versus gate voltage sweep, full measurements of every resonance, and information on the power calibration used in Figure 3. This material is available free of charge via the Internet at <http://pubs.acs.org>.

■ AUTHOR INFORMATION

Corresponding Author

*E-mail: l.p.kouwenhoven@tudelft.nl.

■ ACKNOWLEDGMENTS

We acknowledge B. Giethoorn for fabrication assistance and S. Etaki, G. Götz, and H. Keijzers for discussions. This work was funded by NOW/FOM and SOLID (EU).

■ REFERENCES

- (1) LaHaye, M.; Buu, O.; Camarota, B.; Schwab, K. C. *Science* **2004**, *304*, 74–77.
- (2) O'Connell, A. D.; Hofheinz, M.; Ansmann, M.; Bialczak, R. C.; Lenander, M.; Lucero, E.; Neeley, M.; Sank, D.; Wang, H.; Weides, M.; Wenner, J.; Martinis, J. M.; Cleland, A. N. *Nature* **2010**, *464*, 697–703.
- (3) Rocheleau, T.; Ndukum, T.; Macklin, C.; Hertzberg, J. B.; Clerk, A. A.; Schwab, K. C. *Nature* **2010**, *463*, 72–75.
- (4) Teufel, J. D.; Donner, T.; Li, D.; Harlow, J. W.; Allman, M. S.; Cicak, K.; Sirois, A. J.; Whittaker, J. D.; Lehnert, K. W.; Simmonds, R. W. *Nature* **2011**, *475*, 359–363.
- (5) Safavi-Naeini, A. H.; Chan, J.; Hill, J. T.; Alegre, T. P. M.; Krause, A.; Painter, O. *arXiv.org:1108.4680*, 2011 (accessed September 1, 2011).
- (6) Ekinci, K.; Roukes, M. *Rev. Sci. Instrum.* **2005**, *76*, 061101.
- (7) Huttel, A.; Steele, G.; Witkamp, B.; Poot, M. *Nano Lett.* **2009**, *9*, 2547–2552.
- (8) Steele, G. A.; Huttel, A.; Witkamp, B.; Poot, M.; Meerwaldt, H.; Kouwenhoven, L. P.; van der Zant, H. S. J. *Science* **2009**, *325*, 1103.
- (9) Sazonova, V.; Yaish, Y.; Ustunel, H.; Roundy, D.; Arias, T.; McEuen, P. L. *Nature* **2004**, *431*, 284–287.
- (10) Garcia-Sanchez, D.; Paulo, A. S.; Esplandiu, M. J.; Perez-Murano, F.; Forro, L.; Aguasca, A.; Bachtold, A. *Phys. Rev. Lett.* **2007**, *99*, 085501.
- (11) Lassagne, B.; Tarakanov, Y.; Kinaret, J.; Garcia-Sanchez, D.; Bachtold, A. *Science* **2009**, *325*, 1107–1110.
- (12) Sapmaz, S.; Jarillo-Herrero, P.; Blanter, Y.; Dekker, C.; van der Zant, H. *Phys. Rev. Lett.* **2006**, *96*, 026801.
- (13) Leturcq, R.; Stampfer, C.; Inderbitzin, K.; Durrer, L.; Hierold, C.; Mariani, E.; Schultz, M. G.; von Oppen, F.; Ensslin, K. *Nat. Phys.* **2009**, *5*, 327–331.
- (14) Kuemmeth, F.; Ilani, S.; Ralph, D. C.; McEuen, P. L. *Nature* **2008**, *452*, 448–452.
- (15) Deshpande, V. V.; Chandra, B.; Caldwell, R.; Novikov, D. S.; Hone, J.; Bockrath, M. *Science* **2009**, *323*, 106–110.
- (16) Steele, G. A.; Gotz, G.; Kouwenhoven, L. P. *Nat. Nanotechnol.* **2009**, *4*, 363–367.
- (17) Gouttenoire, V.; Barois, T.; Perisanu, S.; Leclercq, J.-L.; Purcell, S. T.; Vincent, P.; Ayari, A. *Small* **2010**, *6*, 1060–1065.
- (18) Postma, H.; de Jonge, M.; Yao, Z.; Dekker, C. *Phys. Rev. B* **2000**, *62*, 10653–10656.
- (19) Eichler, A.; Chaste, J.; Moser, J.; Bachtold, A. *Nano Lett.* **2011**, *11*, 2699–2703.
- (20) Wu, C.; Zhong, Z. *Appl. Phys. Lett.* **2011**, *99*, 083110.
- (21) Jöckel, A.; Rakher, M. T.; Korppi, M.; Camerer, S.; Hunger, D.; Mader, M.; Treutlein, P. *Appl. Phys. Lett.* **2011**, *99*, 143109.
- (22) Stowe, T.; Yasumura, K.; Kenny, T.; Botkin, D.; Wago, K.; Rugar, D. *Appl. Phys. Lett.* **1997**, *71*, 288–290.
- (23) Sapmaz, S.; Blanter, Y.; Gurevich, L. *Phys. Rev. B* **2003**, *67*, 235414.
- (24) Witkamp, B.; Poot, M.; van der Zant, H. S. J. *Nano Lett.* **2006**, *6*, 2904–2908.
- (25) Poot, M. *Mechanical systems at the nanoscale*. Ph.D. Thesis, TU Delft, 2009.
- (26) Stone, A.; Lee, P. *Phys. Rev. Lett.* **1985**, *54*, 1196–1199.
- (27) Beenakker, C. *Phys. Rev. B* **1991**, *44*, 1646–1656.